Radiology: Cardiothoracic Imaging

ORIGINAL RESEARCH

Lethal COVID-19: Radiologic-Pathologic Correlation of the Lungs

Maurice Henkel, MD • Thomas Weikert, MD • Katharina Marston, MD • Nathalie Schwab, MD • Gregor Sommer, MD, MSc • Jasmin Haslbauer, MD • Fabian Franzeck, MD • Constantin Anastasopoulos, MD • Bram Stieltjes, MD, PhD • Anne Michel, MD • Jens Bremerich, MD, MHBA • Thomas Menter, MD • Kirsten D. Mertz, MD, PhD • Alexandar Tzankov, MD • Alexander W. Sauter, MD

From the Department of Radiology (M.H., T.W., G.S., C.A., B.S., J.B., A.W.S.), Department of Research & Analytic Services (M.H., T.W., F.F., B.S.), and Division of Histopathology and Autopsy, Institute of Pathology (K.M., J.H., T.M., A.T.), University Hospital Basel, University of Basel, Petersgraben 4, 4031 Basel, Switzerland; and Department of Pathology, Cantonal Hospital Baselland, Liestal, Switzerland (M.H., N.S., A.M., K.D.M.). Received June 22, 2020; revision requested July 6; revision received October 23; accepted November 6. **Address correspondence to** T.W. (e-mail: *thomas.weikert@usb.ch*).

Conflicts of interest are listed at the end of this article.

Radiology: Cardiothoracic Imaging 2020; 2(6):e200406 • https://doi.org/10.1148/ryct.2020200406 • Content codes: CH CT

Purpose: The purpose of this retrospective study was to correlate CT patterns of fatal cases of coronavirus disease 2019 (COVID-19) with postmortem pathology observations.

Materials and Methods: The study included 70 lung lobes of 14 patients who died of reverse-transcription polymerase chain reaction–confirmed COVID-19. All patients underwent antemortem CT and autopsy between March 9 and April 30, 2020. Board-certified radiologists and pathologists performed lobewise correlations of pulmonary observations. In a consensus reading, 267 radiologic and 257 histopathologic observations of the lungs were recorded and systematically graded according to severity. These observations were matched and evaluated.

Results: Predominant CT observations were ground-glass opacities (GGO) (59/70 lobes examined) and areas of consolidation (33/70). The histopathologic observations were consistent with diffuse alveolar damage (70/70) and capillary dilatation and congestion (70/70), often accompanied by microthrombi (27/70), superimposed acute bronchopneumonia (17/70), and leukocytoclastic vasculitis (7/70). Four patients had pulmonary emboli. Bronchial wall thickening at CT histologically corresponded with acute bronchopneumonia. GGOs and consolidations corresponded with mixed histopathologic observations, including capillary dilatation and congestion, interstitial edema, diffuse alveolar damage, and microthrombosis. Vascular alterations were prominent observations at both CT and histopathology.

Conclusion: A significant proportion of GGO correlated with the pathologic processes of diffuse alveolar damage, capillary dilatation and congestion, and microthrombosis. Our results confirm the presence and underline the importance of vascular alterations as key pathophysiologic drivers in lethal COVID-19.

Supplemental material is available for this article.

Coronavirus disease 2019 (COVID-19) caused a pandemic with more than 34 million cases worldwide (1). It is caused by severe acute respiratory syndrome coronavirus 2 (SARS-CoV2) and has an estimated mortality rate of up to 5%–10% (2). Given the high reproduction number of the virus, diagnostic tools for rapid diagnosis and evaluation are important to track and mitigate transmission. CT of the chest is sensitive for COVID-19 in high prevalence areas and may have a role in identifying other causes of respiratory failure (3). Frequently found observations include ground-glass opacities (GGOs), consolidations, crazy-paving pattern, reticulations, thickened interlobular septa, and air bronchograms. A better characterization of the main pathologic drivers for each radiologic pattern, which is currently lacking (4,5), could provide a strong, rational foundation for treatment strategies. The first postmortem examination of a patient with COVID-19 (6) showed pulmonary edema and hyaline membrane formation in both lungs, which is the assumed histopathologic correlate of GGO (7). Based on knowledge previously acquired from SARS cases, diffuse alveolar damage is suspected to represent the primary histologic response that accompanies acute lung injury (8). Furthermore, there is new evidence that associates thromboembolic complications in COVID-19 with coagulation activation, endothelial dysfunction, capillary congestion, and acute (exudative) diffuse alveolar damage (DAD) (9–11). Microthrombosis of lung capillary networks and thromboembolism are emerging as key pathophysiologic drivers behind hypoxemia leading to mechanical ventilation (12,13). Radiologic imaging might reflect these vascular abnormalities by the vascular thickening sign (14) and perfusion abnormalities (15).

The purpose of this retrospective study is to gain knowledge on the pathologies underlying CT patterns in COVID-19 by means of radiologic-pathologic correlation analysis of a local COVID-19 autopsy series of patients who underwent antemortem chest CT.

Abbreviations

COVID-19 = coronavirus disease 2019, CTPA = CT pulmonary angiogram, DAD = diffuse alveolar damage, GGO = ground-glass opacities, SARS-CoV-2 = severe acute respiratory syndrome coronavirus 2

Summary

This study deepens our understanding of the pathophysiology of lethal coronavirus disease 2019 by an in-depth pathologic-radiologic correlation analysis and confirms the presence of vascular alterations.

Key Points

- Ground-glass opacities and consolidations in coronavirus disease 2019 correlate with multiple pathologic processes, notably diffuse alveolar damage, capillary dilatation and congestion, and microthrombosis.
- Acute bronchopneumonia is more frequently associated with bronchial wall thickening and consolidation.
- Vascular alterations such as vascular enlargement sign, capillary dilatation and congestion, and microthrombosis are prominent findings at both CT and histopathology.

Materials and Methods

This retrospective dual-center radiology and pathology study was approved by the local ethics committee, and written informed consent was obtained from all subjects (Ethikkommission Nordwest- und Zentralschweiz; EKNZ; project ID 2020-00629).

Study Population

We retrospectively identified all lethal COVID-19 cases confirmed by reverse-transcription polymerase chain reaction with both an antemortem CT and autopsy performed between March 9 and April 30, 2020 (n = 14). In cases with multiple CT examinations, the last antemortem scan was selected for analysis. Complete autopsy was performed in 13 cases and partial autopsy of the upper respiratory tract, lungs, and heart in one case. Autopsies were executed at at the University Hospital Basel, Switzerland (n=10) and Cantonal Hospital Baselland, Switzerland (n=4). Main clinical symptoms and medication were summarized and evaluated.

CT

All patients underwent thin-section, 1-mm chest CT (scanners: Somatom Force [n = 2; 2 × 192 sections], Somatom Definition Edge [n = 2; 128 sections], Somatom Definition AS+ [n = 7; 128 sections], Biograph 128 [n = 1; 128 sections], all Siemens Healthineers; iCT 256 [n = 2; 256 sections], Philips Healthcare). Peak kilovoltage was 80–120 kV (mean, 105 kV ± 11 standard deviation); exposure, 72–498 mAs (mean, 175 mAs ± 142); and section thickness, 1 mm (all cases). Image acquisition was conducted in supine position. Contrast agents were utilized in five cases (iopromide; Bayer); all other scans were without contrast material. Fully anonymized, transverse chest CT series of this cohort in lung kernel reconstruction are hosted on the cloud and are publicly available. The links can be found in the Appendix (supplement).

Two radiologists (G.S. and A.W.S.), each with 12 years of experience in thoracic radiology, performed a consensus reading of the following CT patterns that are common in COVID-19 (16): *(a)* GGO, reticulations, crazy paving, consolidations, bronchial wall thickening, atelectasis, and lymphadenopathy, all as defined by the Fleischner Society Glossary of Terms for Thoracic Imaging (17); and *(b)* vascular thickening, pleural effusion, pulmonary embolism, and pulmonary congestion. Severity was graded lobewise using a four-step scale: none, mild (0%–33% of lobe involved), moderate (34%–66% of lobe involved), and severe (67%–100% of lobe involved). Vascular thickening (vascular enlargement/vascular congestion) and pulmonary arterial enlargement (related to the corresponding bronchus) were rated by means of binary grading (negative/positive). Figure 1, *A* and *B* provide examples of vascular CT radiographic features examined in this study.

Gross Findings

Our institute developed a COVID-19–optimized autopsy protocol in line with recently published recommendations (18). Thoracic organs, lungs, trachea, and larynx were completely exenterated and perfused via the trachea with 4% refrigerated (+4°C) phosphate-buffered formalin (pH 7.4). The trachea was then closed with a clamp, and specimens were left in formalin at room temperature for 72 hours before dissection. The lungs were subsequently cut into 0.5–1-cm parasagittal slices. At least two sections of the first 3 cm of subpleural parenchymal of each lobe, as well as the trachea, were histologically analyzed. The observations were graded in a four-step scale according to severity (none, mild, moderate, severe; Table 1).

Microscopy

Tissue samples were processed using standard laboratory equipment and stained with standard histochemical methods (hematoxylin-eosin staining). The histopathologic specimens were reviewed in consensus by two pathologists with 13 (T.M.) and 20 (A.T.) years of experience. The observations were graded in a four-step scale according to severity (none, mild, moderate, severe; Table 2). Figure 1, *C–H* provide an overview of all histopathologic features examined in this study.

Radiologic-Pathologic Correlation and Statistical Analysis

To ensure the highest possible granularity despite retrospective study design and temporal and local variability of inflammatory processes, the radiologic-pathologic correlation was performed at a lobewise level instead of a patientwise level. The observations of each lobe were recorded separately and graded according to severity (either binary, positive/negative, or a four-step scale, using the terms none, mild, moderate, and severe) in close coordination between radiologists and pathologists. The correlation analysis examined whether radiologic observations were associated with pathologic patterns. In cases that displayed multiple radiologic features within a lobe, features were independently compared between the corresponding gross specimen and the histopathological findings.

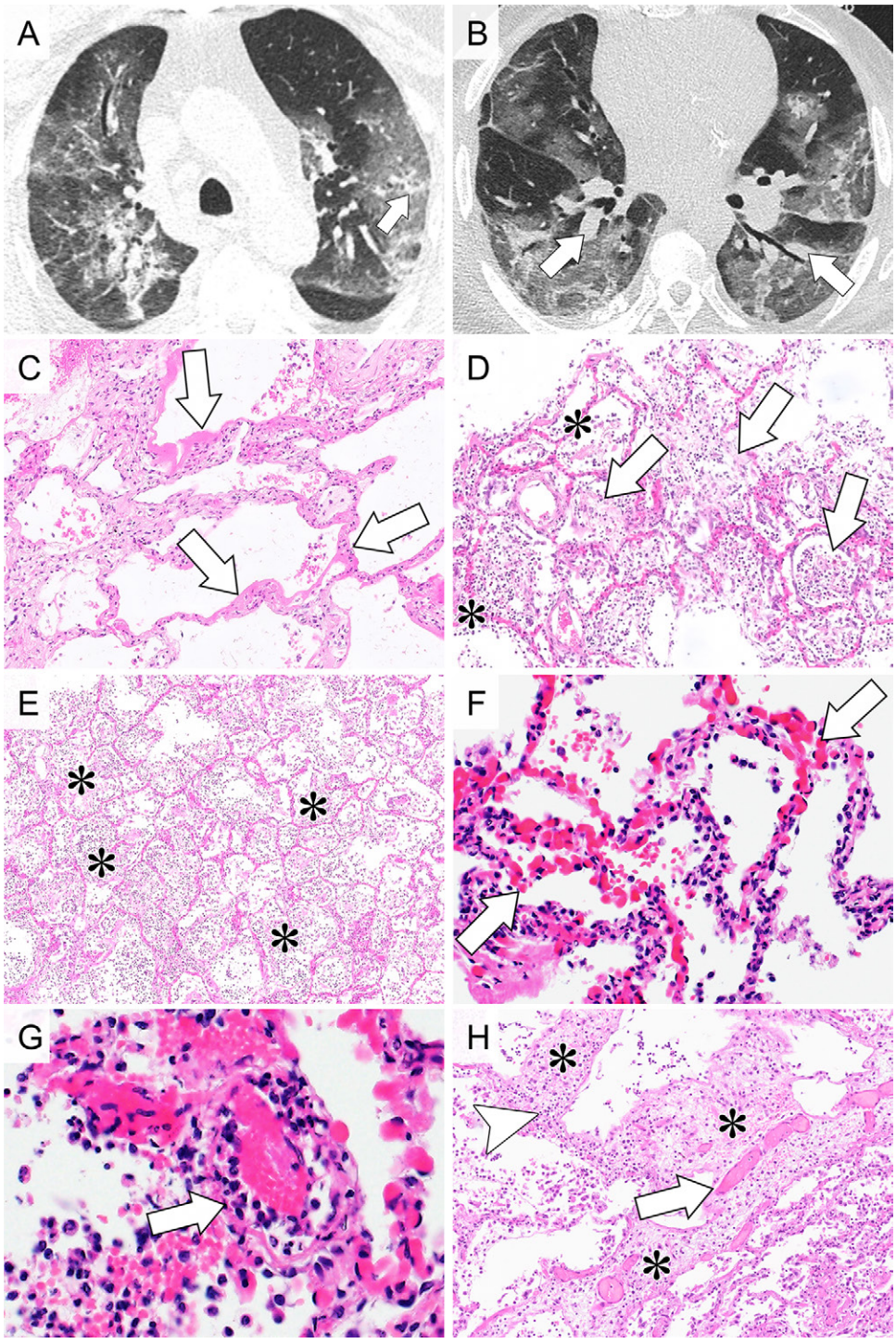

Figure 1: Overview of radiographic and histopathologic observations. *A*, Transverse CT image shows dilated peripheral focal pulmonary artery next to consolidation and ground-glass opacity marked with an arrow (vascular thickening). *B*, Transverse CT image shows dilated segmental arteries marked with arrows (pulmonary arterial enlargement). *C*, Photomicrograph shows diffuse alveolar damage, exudative phase. Hyaline membranes made up of fibrin cover surface of alveolae (arrows). There is only a sparse interstitial inflammatory infiltrate. (Hematoxylin-eosin [H&E] stain; original magnification, x100). *D*, Photomicrograph shows diffuse alveolar damage, proliferative phase. Within alveolae, there are fibrohistiocytic proliferations (arrows); hyaline membranes are already resorbed. Extensive capillary congestion is also found (*). (H&E stain; original magnification, x100). *E*, Photomicrograph shows severe acute bronchopneumonia with alveolae filled with aggregates of neutrophils and fibrin (*). There are no hyaline membranes covering alveolar walls. (H&E stain; original magnification, x50). *F*, Photomicrograph with higher magnification of alveolar walls shows massive capillary congestion. (H&E stain; original magnification, x200). *G*, Photomicrograph of small pulmonary artery shows inflammatory infiltrates primarily consisting of neutrophils infiltrating vessel walls (arrow). (H&E stain; original magnification, x400). *H*, Photomicrograph of interstitial edema. Lung parenchyma with massively widened interstitial spaces shows edema (*), dilated capillaries (arrow), and lymphohistiocytic inflammatory infiltrates (arrowhead) (H&E stain; original magnification, x100).

Continuous variables were analyzed by means and ranges (demographics), means and interquartile ranges (IQRs) (laboratory values) and frequencies (number of lobes with a given feature). To test for differences in observations between patients with a short and long time interval between onset of symptoms and CT (imaging features), and between onset of symptoms and autopsy (histopathology features), patients were assigned to short-interval and long-interval cohorts according to the respective median. Patients having a shorter time interval than the median were assigned to the short interval group, and patients having a longer time interval than the median were assigned to the long interval group. χ^2 tests were conducted to assess differences between long/short interval groups regarding age (*t* test) and sex (χ^2 test). Analysis was conducted in R (19) and figures were produced using ggplot2 (20). *P* values ≤ .05 were considered to be statistically significant.

Table 1: Severity Scoring System for Gross Findings

	Severity Scoring		
Gross Finding	Mild	Moderate	Severe
Hemorrhage	<5% of lobe	5%–50% of lobe	>50% of lobe
Consolidation	<10% of lobe	10%–50% of lobe	>50% of lobe
Emphysema	Palpable	Visible	Bullae
Interstitial edema	<10% of lobe	10%–50% of lobe	>50% of lobe
Pulmonary embolism	Peripheral	Central	…

Table 2: Severity Scoring System of Histologic Findings

	Severity Scoring		
Histologic Finding	Mild	Moderate	Severe
Acute (exudative) DAD	<25% of parenchyma, hyaline membranes with pneumocyte denudation	25%–50% of parenchyma, and/or multinucleated cells	>50% of parenchyma, and/or necrosis
Organizing (proliferative) DAD	<25% of parenchyma, intra-alveolar proliferation of fibroblasts	25%–50% of parenchyma	>50% of parenchyma, thickening of interstitial space
Bronchopneumonia	<10% of parenchyma	10%–50% of parenchyma	>50% of parenchyma
Capillary dilatation and congestion	<10% of parenchyma	10%–50% of parenchyma	>50% of parenchyma
Vasculitis	Present	…	…
Interstitial edema	<10% of parenchyma	10%–50% of parenchyma	>50% of parenchyma

Note.—DAD = diffuse alveolar damage.

Results

Clinical Characteristics

Clinical features including comorbidities and symptoms are listed in Table 3. The mean interval from death to autopsy was 38.5 hours (range, 11.0–97.0 hours), and the mean interval between chest CT and death was 3.7 days (range, 0.0–17.0 days). The average hospitalization time before death was 5.5 days. The mean age in our collective was 76 years (range, 58–96 years); 29% of patients were female. There were no statistically significant differences in age and sex between patients with a short and long time interval between onset of symptoms and CT (age, *P* = .19; sex, *P* = .48) and death (age, *P* = .27; sex, *P* = .73), respectively.

The most prevalent clinical symptoms were cough (*n* = 10), followed by fever (*n* = 7) and dyspnea (*n* = 3). All patients suffered from at least three comorbidities (three comorbidities, *n* = 7; four comorbidities, *n* = 6; more than four comorbidities, *n* = 1 [Table 3]). Patients in our cohort were treated with hydroxychloroquine (*n* = 11), iopinavir/ritonavir (*n* = 7), tocilizumab (*n* = 5), antibiotics (*n* = 4), remdesivir (*n* = 1), or did not receive COVID-19–specific mediation (*n* = 3).

CT

Lobewise analysis resulted in 267 radiologic observations (Fig 2a): GGO (*n* = 59, 14/14 [100%] patients), vascular thickening (*n* = 36, 12/14 [86%] patients), pulmonary arterial enlargement (*n* = 36, 12/14 [86%] patients), consolidations (*n* = 33, 11/14 [79%] patients), bronchial wall thickening (*n* = 32, 8/14 [57%] patients), reticulations (*n* = 23, 8/14 [57%] patients), crazy paving (*n* = 13, 4/14 [29%] patients), atelectasis (*n* = 12, 7/14 [50%] patients), pleural effusion (*n* = 9, 6/14 [43%] patients), lymphadenopathy (*n* = 7, 7/14 [50%] patients), pulmonary embolism (*n* = 5, 1/5 patients with contrast-enhanced CT), and pulmonary congestion (*n* = 2, 1/14 [7%] patients). Anonymized CT scans of all patients are hosted on our freely accessible e-learning server. Links are provided in the Appendix (supplement).

Table 3: Clinical Features Including Comorbidities and Symptoms

Parameter	Value
Clinical Characteristic*	
Age (y)	76 (58–96)
Sex†	M 10 (71.0): F 4 (29.0)
Time between CT and death (d)	3.7 (0–17)
Hospitalization (d)	5.5 (0–17)
Postmortem interval (h)	38.5 (11–97)
Mechanical ventilation	4 of 14 patients
Anticoagulation (prophylactic/ Therapeutic ratio)	8: 6
Comorbidities†	
Hypertension	14 (100.0)
Cardiovascular disease	7 (50.0)
(Pre)obesity	6 (42.8)
Diabetes mellitus, type 2	4 (28.6)
Initial clinical presentation†	
Cough	10 (71.4)
Fever	7 (50.0)
Dyspnea	3 (21.4)
Laboratory values‡	
IL-6 (ng/l)	781 (399–2668)
CRP (mg/l)	248 (136–319)
Ferritin (µg/l)	3086 (2259–4113)
PCT (µg/l)	1.19 (0.10–3.64)
cTnT (ng/l)	33 (18–55)
LDH pg/mL	602 (360–776)

Note.—Listed values correspond to the highest (LDH, cTnT), latest (IL-6, ferritin, PCT, CRP) and, in case of administration of tocilizumab, last CRP value before administration. cTnT = troponin T, CRP = C-reactive protein, IL-6 = interleukin-6, LDH = lactate dehydrogenase, PCT = procalcitonin.
*Except where otherwise noted, data are means with ranges in parentheses.
†Data are numbers with percentages in parentheses
‡Data are medians with interquartile ranges in parentheses.

Time Interval between Onset of Symptoms and CT

The mean interval from first symptoms to CT was 5.7 days. The comparison of patients with a short (n = 9) versus long (n = 5) interval from first symptoms to CT showed varying incidence of multiple radiologic observations (Fig 2b). The differences were statistically significant for bronchial wall thickening (+12.9%, $P < .001$), pulmonary arterial enlargement (+4.1%, P value = .05), and pulmonary embolism (+ 5.0%, P = .003).

Gross Pathology

The overall gross findings of all lobes in all patients are shown in Table 4. Overall presence per patient was heterogeneous and as follows: interstitial edema of interlobular septae (n = 65, 13/14 [93%] patients), areas of consolidation (n = 43, 10/14 [71%] patients), emphysema (n = 13, 7/14 [50%] patients), hemorrhage (n = 9, 5/14 [36%] patients), and pulmonary embolism (n = 9, 4/14 [29%] patients). In all cases, lung parenchyma was heavy and firm and unevenly bluish red with signs of severe congestion.

Histopathology

In the overall lobewise analysis of our examined collective, 257 pathologic observations were recorded (Fig 3a). Observations included capillary dilatation and congestion (n = 70, 14/14 [100%] patients), acute (exudative) phase DAD (n = 54, 11/14 [79%] patients) and organizing (proliferative) phase DAD (n = 26, 7/14 [50%] patients), interstitial edema (n = 64, in 14/14 [100%] patients), superimposed acute bronchopneumonia (n = 17, 7/14 [50%] patients), microthrombi (n = 27, 7/14 [50%] patients), and leukocytoclastic vasculitis (n = 7, 3/14 [21%] patients). Leukocytoclastic vasculitis showed the presence of neutrophils in the vessel wall and was primarily interpreted in the context of severe acute bronchopneumonia; no patient had evidence of generalized systemic vasculitis. Anonymized high-resolution scans of histology sections of each patient with representative lung observations are hosted on a local server and are available online. Links can be found in Appendix E1 (supplement).

Time Interval between Symptom Onset and Death

The mean interval between symptom onset and death was 10.4 days. The comparison of patients with a short (n = 7) versus long (n = 7) interval between symptom onset and death showed varying incidence of histopathologic observations (Fig 3b). There were statistically significantly higher frequencies of acute (exudative) phase DAD (P = .04) and interstitial edema (P = .03) in the short-interval group.

Radiologic-Pathologic Correlation of Pulmonary Observations

When correlating the summed CT features with histopathology of all lobes, the areas of GGO (n = 59 lobes/14 patients) reflected the presence of multiple pathologic processes (Fig 4). Figures 5 and 6 display typical observations in COVID-19, each depicted at gross pathology (left column), CT (middle column), and microscopy (right column). Acute (exudative) phase DAD was observed in 46 (see also Figs 5a–5c, 6a, 6c), organizing (proliferative) phase DAD in 21 (see Figs 5b, 6a, 6c), acute bronchopneumonia in eight (see Figs 5a, 6b), capillary dilatation and congestion in 57 (see Figs 5a–5c, 6a–6c), leukocytoclastic vasculitis in six (see Fig 6b), interstitial edema in 53, and microthrombi in 22 (see Fig 5a) of the 59 lobes presenting GGO. Consolidations at CT (n = 33 lobes/11 patients) were microscopically characterized by multiple pathologic processes of acute (exudative) phase DAD in 21, organizing (proliferative) phase DAD in eight, acute bronchopneumonia in four, capillary dilatation and congestion in 31, leukocytoclastic vasculitis in four, interstitial edema in 29, and microthrombi in 14 of the 33 lobes presenting consolidations. A subanalysis of lobes with pure GGO and consolidation at CT also showed heterogeneous histopathologic patterns including exudative DAD, organizing (proliferative) DAD, acute

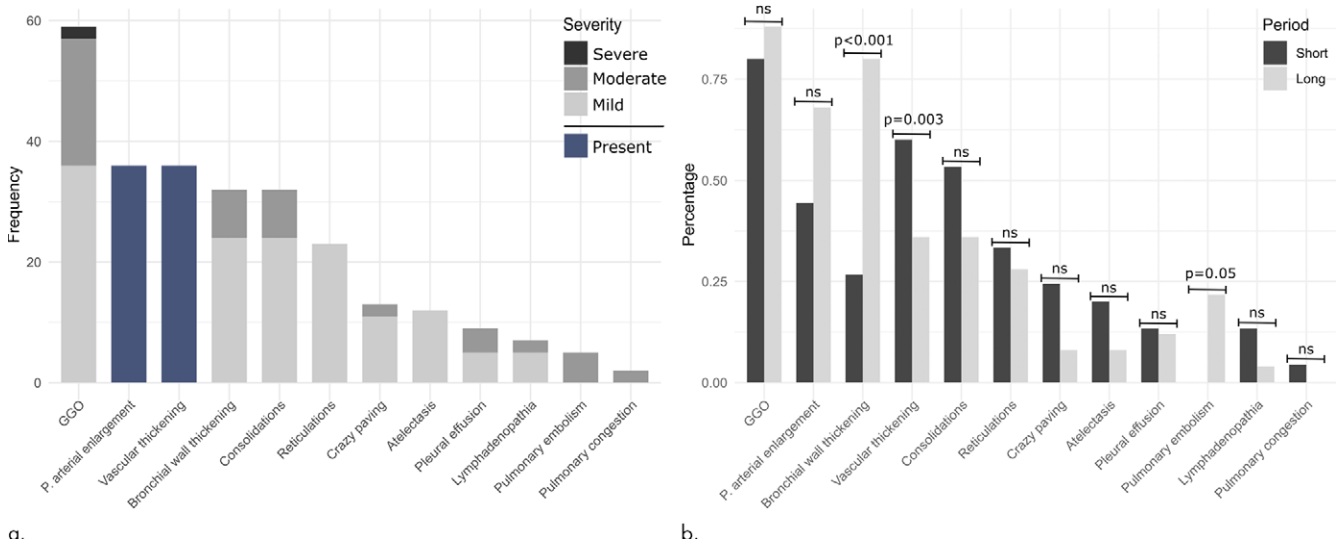

Figure 2: **(a)** Frequencies of lobewise analysis of radiologic findings according to severity grading (in gray) and binary categories (present/absent) for the pulmonary arterial enlargement and vascular thickening sign (in blue). **(b)** Percentage of radiologic findings according to the time interval between onset of symptoms and CT. *P* values are provided if significant. Percentage defined as ratio of lobes with a given feature in relation to all lobes within the time interval category. GGO = ground-glass opacities, P = pulmonary, ns = not significant.

bronchopneumonia, and capillary dilatation and congestion. The comparison of lobes with pathologically defined acute bronchopneumonia versus without revealed consolidations in 58.8% versus 40.4% of lobes and bronchial wall thickening in 47.1% versus 42.0% of lobes, respectively.

Patients with consolidations (n = 11) at CT showed a shorter time to death (2.7 days) compared with those without (n = 3, 7.3 days). When comparing histologic observations in patients with and without consolidations, DAD was more frequent in cases without consolidations (+13.5%), whereas acute bronchopneumonia (+4.6%) and leukocytoclastic vasculitis (+3.6%) were more frequent in cases with consolidations.

Table 4: Overall Gross Pathology Findings of All Lobes in All Patients

Finding	Total	Mild	Moderate	Severe
Interstitial edema	50	6	42	2
Consolidation	43	33	5	5
Emphysema	13	8	5	0
Hemorrhage	9	7	2	0
Pulmonary embolism	9	4	5	0

Note.—Data are numbers of findings.

Discussion

This is the first systematic morphologic comparison of antemortem chest CT scans with postmortem gross findings and histopathology in COVID-19. CT patterns of COVID-19 were characterized by GGO, consolidation, and bronchial and vascular changes. Gross findings included severe interstitial edema and congestion resulting in increased parenchymal consistency, while histologic examination revealed prominent capillary dilatation and congestion with or without microthrombosis, interstitial edema, and DAD as the most consistent finding. Correlations of radiologic and pathologic observations showed that CT patterns reflect multiple pathologic processes of varying composition. All histologic changes investigated were found in GGO as well as in consolidations. Consolidations and bronchial wall thickening were more frequently observed in presence of acute bronchopneumonia, and pulmonary arterial enlargement might be an indicator of microangiopathic change.

Our results showed predominantly bilateral areas of GGO and consolidations, consistent with previous reports on the occurrence of various pulmonary CT observations in COVID-19 (19–21). Radiologic-pathologic correlation showed that CT observations were characterized by multiple pathologic processes of DAD, interstitial edema, and capillary dilatation and congestion. These changes are consistent with previously published studies without detailed CT correlation (10).

While most recent studies also described the radiologic pattern of organization of pneumonia in patients with COVID-19 (4,21), no histopathologic features for fibrosis were found in our study. Interestingly, in a recent study using postmortem transbronchial lung cryobiopsy from six patients with a median illness duration of 32 days, three showed late/fibrotic phase diffuse alveolar damage, one of them with honeycombing (22). In another study, for five patients, who died around 20 days after the beginning of symptoms, the histologic pattern was an acute fibrinous and organizing pneumonia (23). The various radiologic patterns showed only minor differences in the frequency of underlying histopathological changes. The most important components for GGO were capillary dilatation and congestion (26.9%), interstitial edema (25.0%), and acute (exudative) DAD (21.7%). Consolidation showed similar histopathologic patterns with slightly more microthrombosis (12.6% vs 10.4%) and leukocytoclastic vasculitis (3.6% vs 2.4%). Importantly, the observed CT patterns were not linked to a specific histopathologic finding.

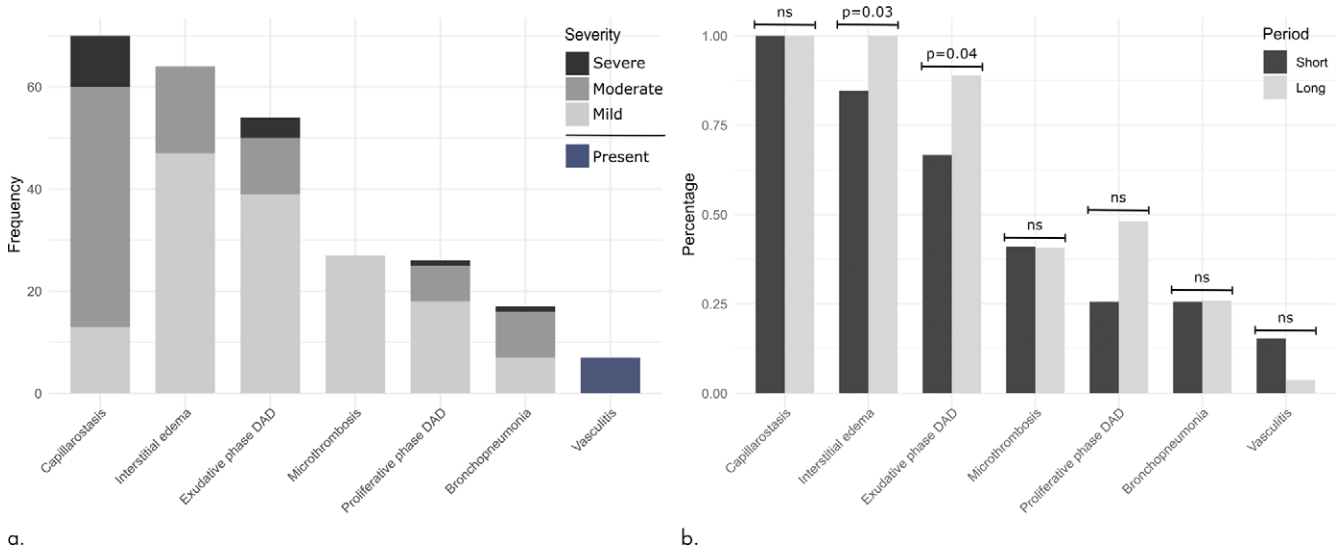

Figure 3: **(a)** Frequencies of lobewise analysis of microscopy findings according to severity grading (in gray) and presence of for vasculitis (in blue). **(b)** Percentage of histopathologic findings according to the time interval between onset of symptoms and autopsy. Percentage defined as ratio of lobes with a given feature in relation to all lobes within the time interval category. *P* values are provided if significant. DAD = diffuse alveolar damage, ns = not significant.

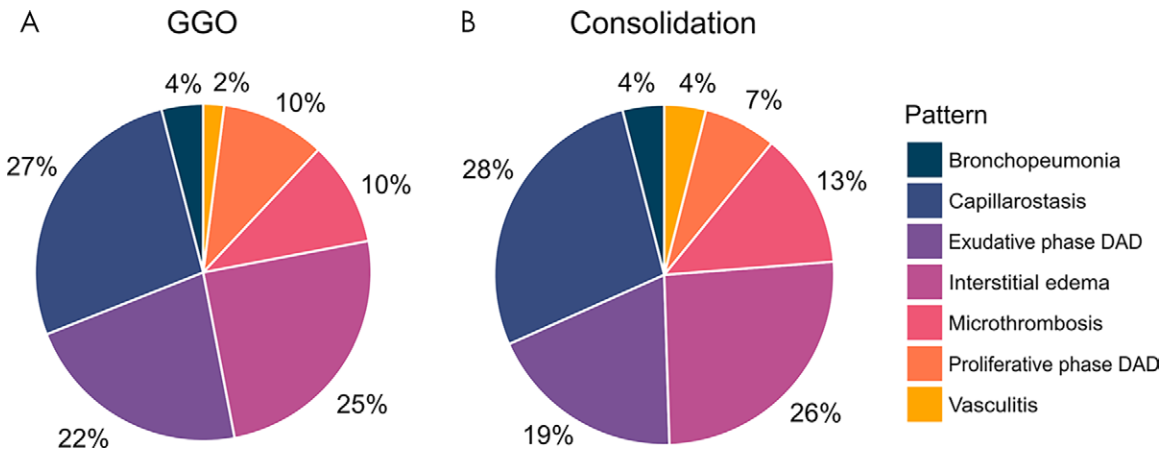

Figure 4: Frequencies of observed histopathologic findings in lobes affected by consolidations and GGO. Consolidations were observed in 33 lobes/11 patients. GGOs were observed in 59 lobes/14 patients. DAD = diffuse alveolar damage, GGO = ground-glass opacity.

Furthermore, an increase in the frequencies of bronchial wall thickening, pulmonary arterial enlargement, and pulmonary embolism in patients with longer symptom onset to CT was found. The increase in bronchial wall thickening and consolidation might be explained by superimposed bacterial superinfections and subsequent acute bronchopneumonia, which was evident in our collective. Figure 5a provides an example. Of note, while there were no evident temporal dynamics of microthrombosis, more pulmonary emboli were detected in patients with a longer interval between onset of symptoms and CTPA in our cohort. Surprisingly, the temporal dynamic of radiographic changes could not be clearly correlated with corresponding histopathologic results. Further evaluation of the histopathologic observations as a function of disease duration showed an increase of acute (exudative) and organizing (proliferative) phase DAD, whereas no fibrotic changes were observed.

The observation of enlarged pulmonary arteries in our series might be related to an increase of parenchymal and predominantly intravascular pressure (24), due to the severe COVID-19 pulmonary microangiopathy affecting the alveolar capillary network (25). In the context of recent reports of pathologically altered coagulation, these results may also indicate an increase in vascular incidents (10,26). Thirty of 388 patients in the study by Lodigiani et al underwent CTPA confirming pulmonary embolism in 10 cases (9). Although higher, this positive rate of 33% seems in line with the observed rate in our collective of 20%; importantly, all our patients received anticoagulation therapy. While most of the currently available literature relies on non–contrast-enhanced CT (27), the need to assess vascular abnormalities is being recognized as an increasingly important factor (28,29), both to distinguish COVID-19 pneumonia from other viral infections and to exclude pulmonary embolism. Interestingly, the high incidence of microthrombosis and the low

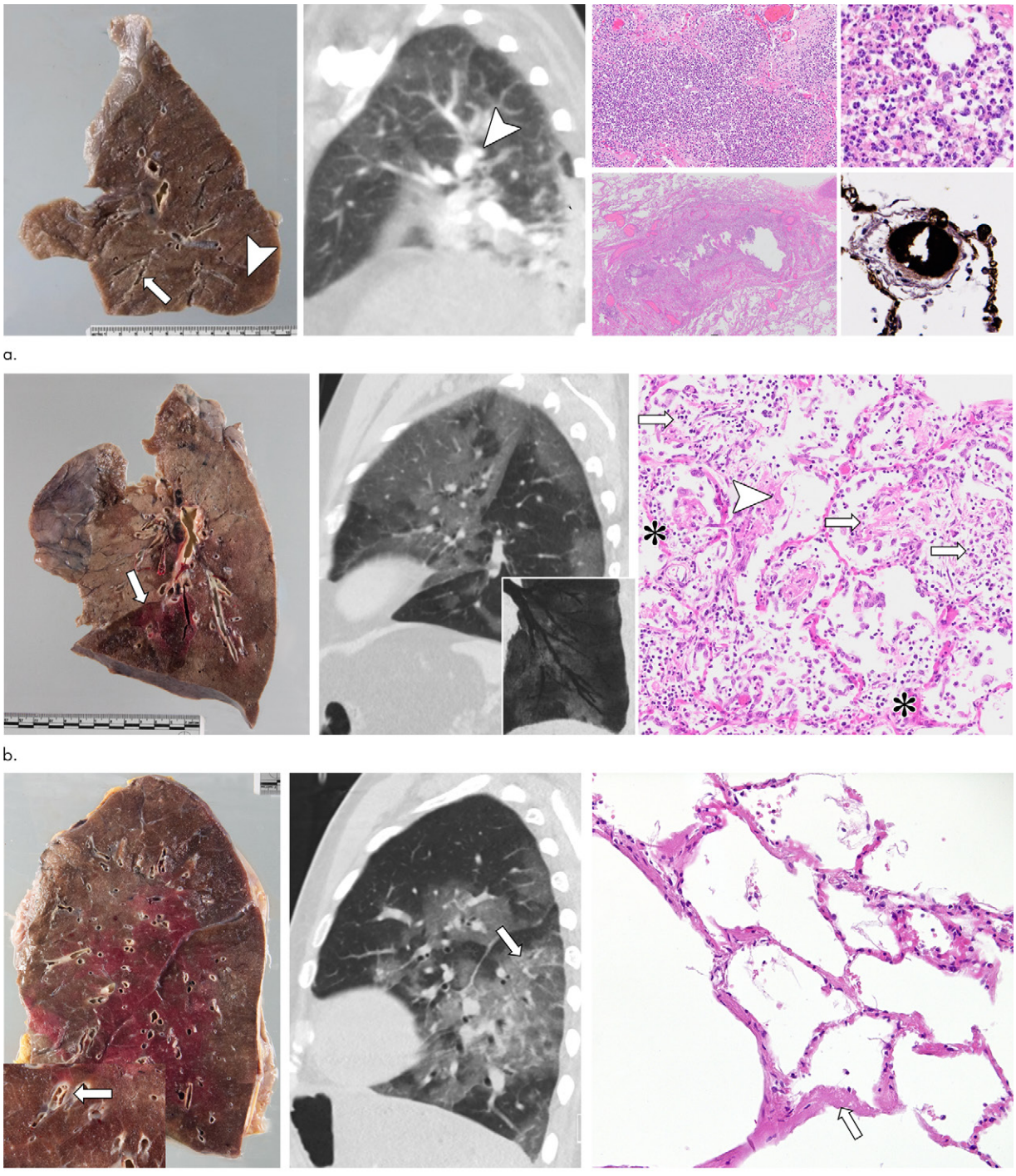

Figure 5: **(a)** Radiologic-pathologic correlation in patient 1, a 67-year-old woman. Gross pathology findings show interlobular septal edema, congestion, thickened bronchial walls (arrow), and consolidation (arrowhead). The corresponding CT in sagittal plane discloses bronchial wall thickening (arrow) and dystelectasis in the posterior parts of the lower lobes (arrowhead). Photomicrographs show bronchopneumonia in the left lower lobe (top left and right), thickened bronchial walls (bottom left), and microthrombosis (bottom right, immunohistochemistry for fibrin polyclonal antibody [A0080; Dako]; other photomicrographs, hematoxylin-eosin [H&E] stain, magnification not available [N/A]). **(b)** Radiologic-pathologic correlation in patient 2, a 66-year-old man. Gross findings document interlobular septal edema and segmental hemorrhage in the anterobasal segment of the left lower lobe (arrow), while CT scan shows peripherally pronounced ground-glass opacity (GGO) in the left lower lobe. Inserted minimum intensity projection reveals some focal bronchial dilatation in association to GGOs. Photomicrograph reveals hyaline membranes as remnants of acute exudative (arrowhead) and intra-alveolar fibroblastic proliferations as signs of proliferative diffuse alveolar damage (DAD) (arrows) . Furthermore, capillaries show extensive congestion (*). (H&E stain, magnification N/A.) **(c)** Radiologic-pathologic correlation in patient 3, a 73-year-old man. Gross findings show interstitial edema, congestion, and chronic pulmonary embolism in the left upper lobe that was not disclosed by imaging due to unenhanced acquisition (insert). CT scan discloses extensive GGO in transition to consolidation in the left lower lobe (arrow) as well as lingula. Photomicrograph reveals hyaline membranes as a correlate of acute exudative DAD predominantly in the left lower lobe (arrow). (H&E stain, magnification N/A.)

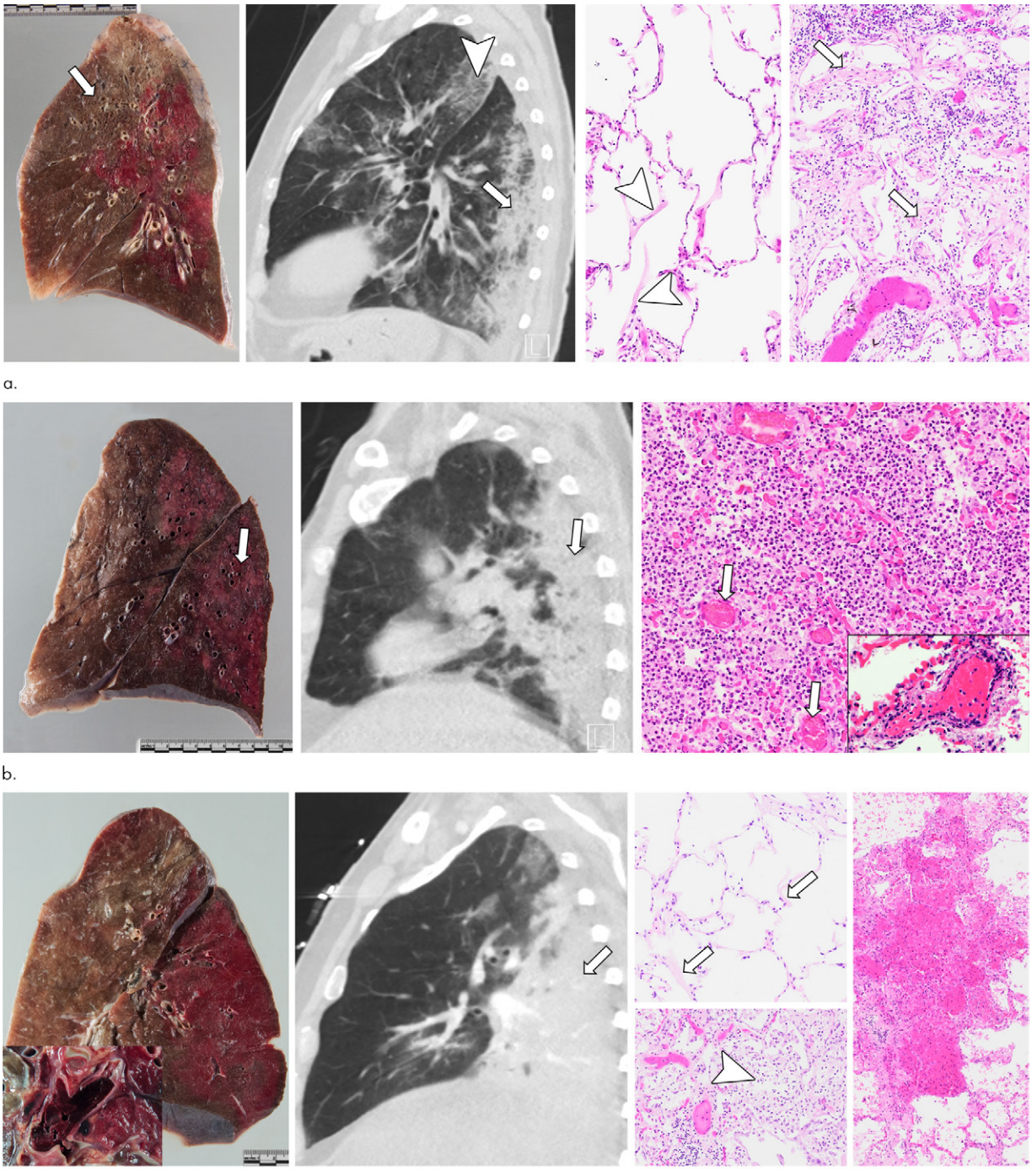

Figure 6: **(a)** Radiologic-pathologic correlation in patient 4, an 81-year-old woman. Gross specimen shows congestion, interlobular septal edema, and emphysema (arrow). CT scan reveals consolidation (arrow) in the posterior parts of the left lower lobe and crazy paving (arrowhead) in the apical upper lobe. Photomicrograph reveals both hyaline membranes as correlates of acute exudative (arrowheads) and intra-alveolar fibrohistiocytic proliferates as signs of proliferative diffuse alveolar damage (DAD) (arrows). (Hematoxylin-eosin [H&E] stain, magnification not available [N/A].) **(b)** Radiologic-pathologic correlation in patient 6, a 71-year-old man. Gross specimen shows congestion and severe consolidation (arrow). CT scan shows obstruction and consolidation in the posterior parts of the upper and lower right lobe (arrow). Photomicrograph shows extensive bronchopneumonia, dilated capillaries (arrows), vasculitis (insert at bottom right), and microthrombosis (not shown). Next-generation sequencing identified bacterial species such as *Staphylococcus aureus* and several strains of streptococcal species. (H&E stain, magnification N/A.) **(c)** Radiologic-pathologic correlation in patient 9, a 58-year-old man. Gross specimen shows congestion, interlobular septal edema, and multiple thromboembolisms (insert at lower left). CT scan reveals subtotal consolidation of the left lower lobe (arrow) and bilateral pulmonary embolisms (not shown). Photomicrograph shows hyaline membranes as correlates of acute exudative (arrows) and fibroblastic proliferations as signs of proliferative DAD (arrowhead), as well as alveolar hemorrhage (far right). (H&E stain, magnification N/A.)

number of pulmonary emboli detected with CTPA suggest a possible underestimation of the vascular alterations associated with COVID-19 using imaging, especially in unenhanced scans. Newly described signs such as "vascular thickening," "pulmonary arterial enlargement," or "vascular congestion" could reflect these alterations. Severe influenza pneumonia has previously been described to cause a hyperinflammatory response with virally associated platelet activation, which can lead to pulmonary thrombosis with passive congestion. Similar to influenza pneumopathy, COVID-19 is able to limit compensatory ventilation responses by means of vascular leakage and alveolar edema, thus contributing to widespread hemorrhage (10,30). According to a comparative autopsy study, alveolar capillary microthrombi were nine times as prevalent in patients with COVID-19 as in patients with influenza, and extent of angiogenesis was 2.7 times higher than in influenza (25). Therefore, described vascular alterations seem to be specific for COVID-19.

Our study has several limitations. First, its retrospective design and the relatively small number of cases. For this reason, no complex statistical analyses have been performed. Second, the time intervals between symptoms, CT, and autopsy varied. This is a factor that cannot be controlled in an observational study. Third, as all patients died of COVID-19, there was a bias toward more severe and rapidly progressive courses of disease. Fourth, the correlation analysis was performed on a per-lobe level. A finer granularity was not possible due to the specific COVID-19 autopsy protocol. For future studies, image-guided tissue sampling is desirable to further increase the resolution of analysis. However, as stated in the results, multiple pathologic processes were found also in lobes with pure GGO/consolidation patterns at CT. Finally, CT parameters and vendors differed due to the dual-center nature of this study. However, all scans were acquired with a high diagnostic quality clearly suitable for this correlation analysis as shown in supplementary materials.

The results of this study deepen our understanding of COVID-19 pathophysiology confirming the importance of vascular alterations. Our observations imply that both severe acute lung injury and vascular complications contribute to fatal outcomes. Therefore, therapy optimization must focus on both pathologies to improve clinical management of COVID-19.

Acknowledgments: We thank all patients and their families for their willingness to dedicate the bodies to the department of pathology for autopsy. A.T. received funding from the Botnar Research Center for Child Health (Fast Track Call). We thank Rita Achermann (statistician) for statistical advice.

Author contributions: Guarantor of integrity of entire study, M.H., J.B., K.D.M., A.T., A.W.S.; study concepts/study design or data acquisition or data analysis/interpretation, all authors; manuscript drafting or manuscript revision for important intellectual content, all authors; approval of final version of submitted manuscript, all authors; agrees to ensure any questions related to the work are appropriately resolved, all authors; literature research, M.H., T.W., K.M., J.H., F.F., C.A., A.M., K.D.M., A.T., A.W.S.; clinical studies, M.H., K.M., N.S., G.S., A.M., T.M., K.D.M., A.T., A.W.S.; statistical analysis, M.H., T.W., A.M., A.W.S.; and manuscript editing, all authors

Disclosures of Conflicts of Interest: **M.H.** disclosed no relevant relationships. **T.W.** disclosed no relevant relationships. **K.M.** disclosed no relevant relationships. **N.S.** disclosed no relevant relationships. **G.S.** disclosed no relevant relationships. **J.H.** Activities related to the present article: disclosed grant to author's institution from Botnar Research Centre for Child Health.no relevant relationships. Activities not related to the present article: disclosed no relevant relationships. Other relationships: disclosed no relevant relationships. **F.F.** disclosed no relevant relationships. **C.A.** disclosed no relevant relationships. **B.S.** disclosed no relevant relationships. **A.M.** disclosed no relevant relationships. **J.B.** disclosed no relevant relationships. **T.M.** disclosed no relevant relationships. **K.D.M.** disclosed no relevant relationships. **A.T.** Activities related to the present article: disclosed grant to author's institution from Botnar Research Centre for Child Health. Activities not related to the present article: disclosed no relevant relationships. Other relationships: disclosed no relevant relationships. **A.W.S.** disclosed no relevant relationships.

References

1. Johns Hopkins University & Medicine. Coronavirus Resource Center. https://coronavirus.jhu.edu/map.html. Updated September 29, 2020. Accessed October 1, 2020.
2. Wilson N, Kvalsvig A, Barnard LT, Baker MG. Case-Fatality Risk Estimates for COVID-19 Calculated by Using a Lag Time for Fatality. Emerg Infect Dis 2020;26(6):1339–1441.
3. American College of Radiology. ACR recommendations for the use of chest radiography and computed tomography (CT) for suspected COVID-19 infection. https://www.acr.org/Advocacy-and-Economics/ACR-Position-Statements/Recommendations-for-Chest-Radiography-and-CT-for-Suspected-COVID19-Infection. Updated March 22, 2020. Accessed October 1, 2020.
4. Kay F, Abbara S. The Many Faces of COVID-19: Spectrum of Imaging Manifestations. Radiol Cardiothorac Imaging 2020;2(1):e200037.
5. Kanne JP, Little BP, Chung JH, Elicker BM, Ketai LH. Essentials for Radiologists on COVID-19: An Update—Radiology Scientific Expert Panel. Radiology 2020;296(2):E113–E114.
6. Xu Z, Shi L, Wang Y, et al. Pathological findings of COVID-19 associated with acute respiratory distress syndrome. Lancet Respir Med 2020;8(4):420–422.
7. Ye Z, Zhang Y, Wang Y, Huang Z, Song B. Chest CT manifestations of new coronavirus disease 2019 (COVID-19): a pictorial review. Eur Radiol 2020;30(8):4381–4389.
8. Wu J, Wu X, Zeng W, et al. Chest CT Findings in Patients With Coronavirus Disease 2019 and Its Relationship With Clinical Features. Invest Radiol 2020;55(5):257–261.
9. Lodigiani C, Iapichino G, Carenzo L, et al. Venous and arterial thromboembolic complications in COVID-19 patients admitted to an academic hospital in Milan, Italy. Thromb Res 2020;191:9–14.
10. Wichmann D, Sperhake JP, Lütgehetmann M, et al. Autopsy Findings and Venous Thromboembolism in Patients With COVID-19: A Prospective Cohort Study. Ann Intern Med 2020;173(4):268–277.
11. Menter T, Haslbauer JD, Nienhold R, et al. Postmortem examination of COVID-19 patients reveals diffuse alveolar damage with severe capillary congestion and variegated findings in lungs and other organs suggesting vascular dysfunction. Histopathology 2020;77(2):198–209.
12. Cui S, Chen S, Li X, Liu S, Wang F. Prevalence of venous thromboembolism in patients with severe novel coronavirus pneumonia. J Thromb Haemost 2020;18(6):1421–1424.
13. Escher R, Breakey N, Lämmle B. Severe COVID-19 infection associated with endothelial activation. Thromb Res 2020;190:62.
14. Qanadli SD, Rotzinger DC. Vascular Abnormalities as Part of Chest CT Findings in COVID-19. Radiol Cardiothorac Imaging 2020;2(2):e200161.
15. Lang M, Som A, Mendoza DP, et al. Hypoxaemia related to COVID-19: vascular and perfusion abnormalities on dual-energy CT. Lancet Infect Dis 2020. 10.1016/S1473-3099(20)30367-4. Published online April 30, 2020.
16. Gozansky EK, Moore WH. SARS-CoV-2 From the Trenches: A Perspective From New York City. AJR Am J Roentgenol 2020;215(1):27–28.
17. Hansell DM, Bankier AA, MacMahon H, McLoud TC, Müller NL, Remy J. Fleischner Society: glossary of terms for thoracic imaging. Radiology 2008;246(3):697–722.
18. Hanley B, Lucas SB, Youd E, Swift B, Osborn M. Autopsy in suspected COVID-19 cases. J Clin Pathol 2020;73(5):239–242.
19. R Core Team. R: A language and environment for statistical computing. Vienna, Austria: R Foundation for Statistical Computing, 2014.
20. Wickham H. ggplot2: elegant graphics for data analysis. 2nd ed. Cham, Switzerland: Springer, 2016.
21. Wu Y, Xie Y, Wang X, Longitudinal CT. Findings in COVID-19 Pneumonia: Case Presenting Organizing Pneumonia Pattern. Radiol Cardiothorac Imaging 2020;2(1):e200031.
22. Barisione E, Grillo F, Ball L, et al. Fibrotic progression and radiologic correlation in matched lung samples from COVID-19 post-mortems. Virchows Arch 2020. 10.1007/s00428-020-02934-1. Published online September 28, 2020.

23. Gattinoni L, Chiumello D, Caironi P, et al. COVID-19 pneumonia: different respiratory treatments for different phenotypes? Intensive Care Med 2020;46(6):1099–1102.
24. Raymond TE, Khabbaza JE, Yadav R, Tonelli AR. Significance of main pulmonary artery dilation on imaging studies. Ann Am Thorac Soc 2014;11(10):1623–1632.
25. Ackermann M, Verleden SE, Kuehnel M, et al. Pulmonary Vascular Endothelialitis, Thrombosis, and Angiogenesis in Covid-19. N Engl J Med 2020;383(2):120–128.
26. Klok FA, Kruip MJHA, van der Meer NJM, et al. Confirmation of the high cumulative incidence of thrombotic complications in critically ill ICU patients with COVID-19: An updated analysis. Thromb Res 2020;191:148–150.
27. Rubin GD, Ryerson CJ, Haramati LB, et al. The Role of Chest Imaging in Patient Management During the COVID-19 Pandemic: A Multinational Consensus Statement From the Fleischner Society. Chest 2020;158(1):106–116.
28. Grillet F, Behr J, Calame P, Aubry S, Delabrousse E. Acute Pulmonary Embolism Associated with COVID-19 Pneumonia Detected with Pulmonary CT Angiography. Radiology 2020;296(3):E186–E188.
29. Léonard-Lorant I, Delabranche X, Séverac F, et al. Acute Pulmonary Embolism in Patients with COVID-19 at CT Angiography and Relationship to d-Dimer Levels. Radiology 2020;296(3):E189–E191.
30. Yang Y, Tang H. Aberrant coagulation causes a hyper-inflammatory response in severe influenza pneumonia. Cell Mol Immunol 2016;13(4):432–442.